Supporting information for :

Multi-Channel smFRET study reveals a Compact conformation of EF-G on the Ribosome

This supplemental material contains materials and preparation details, 2 supplement table, and 15 supplemental figures.

Table of content:

MATERIALS AND PREPARATIONS

Protein mutagenesis and expression. BL21 Star (DE3)pLysS and BL21(DE3)pLysE competent cells, and GeneArt Site-directed Mutagenesis PLUS Kit were purchased from ThermoFisher Scientific. Q5 Site-directed Mutagenesis Kit was purchased from New England Biolabs. The HisTrap™ HP 5 ml column and Nap™ desalting columns were acquired from Cytiva. Amicon Ultra centrifugal filters are from Millipore.

Sarcin-ricin loop RNA oligo of 29 nt and biotinylated at the 5'-end (5'-biotin-TEG-CUGCUCCUAG UACGAGAGGA CCGGAGUGG) was purchased from Integrated DNA Technologies.

Fluorescent Dyes and mant-nucleotide. Alexa Fluor™ 488 C_5 maleimide (Alexa 488) and Alexa Fluor™ 594 C_5 maleimde (Alexa 594) fluorescent dyes were purchased from ThermoFisher Scientific, Cyanine3 maleimide (Cy3) and Cyanine5 maleimide (Cy5) fluorescent dyes were purchased from Lumiprobe. 2'/3'-O-(N-Methyl-anthraniloyl)-guanosine-5'-triphosphate (mant-GTP) and 2'/3'-O-(N-Methyl-anthraniloyl)-guanosine-5'-diphosphate (mant-GDP) were from Sigma Aldrich.

All the other materials were from Millipore-Sigma.

mRNA preparation. The DNA template oligos for the *in vitro* T7 transcription reaction were purchased from Integrated DNA Technologies. The HiScribe T7 High-Yield RNA Kit was from New England Biolabs. The 70-nt mRNA (5'-GGGCAACUGU UAAUUAAAUU AAAUUAAAAA GGAAAUAAAA AUGUUUAAAC GUAAAUCUAC UGCUGAACUC-3') with a ribosome-binding site and a 10-codon-long non-stop coding sequence for Met-Phe-Lys-Arg-Lys-Ser-Thr-Ala-Glu-Leu peptide was synthesized and purified according to manufacturer's instructions.

Ribosome preparation. The 70S ribosomes were purified from *E. coli* MRE600 according as previously described.(1) A culture of *E. coli* MRE600 was propagated in LB medium in a shaker incubator at 37°C and 200 rpm until optical density at 600 nm reached value of 0.6. The cells were harvested by centrifugation at 3,000xg, 4°C, for 20 min. The cell pellet was washed with cold buffer I (50 mM Tris-HCl, pH 7.6, 10 mM $MgCl_2$, 100 mM NH_4Cl, 6 mM BME, 0.5 mM EDTA). Then the cells were resuspended in the same buffer with 0.2 mg/ml egg white lysozyme and 2 μg/ml DNase I and incubated for 30 min on ice. Afterward the cells were lysed by sonication for 5

min (10 sec pulse, 20 sec pause) on ice. Cell debris were removed by two consecutive centrifugations at 14,500xg, 4°C, for 1 hour each. Cleared supernatant was layered on top of pre-cooled 1.1 M sucrose cushion in buffer II (20 mM Tris-HCl, pH 7.6, 10 mM $MgCl_2$, 500 mM NH_4Cl, 6 mM BME, 0.5 mM EDTA) with volume ratio 1:1, respectively. The ribosomes were pelleted by centrifugation on Beckman XL-80 ultracentrifuge with Type 45 Ti Fixed-Angle rotor at 120,000xg, 4°C, for 20 hours. The collected pellet was carefully rinsed with buffer I, then the ribosomes were resuspended in the same buffer, and the concentration of NH_4Cl was adjusted to 400 mM. The ribosomes were pelleted again by ultracentrifugation at 120,000xg, 4°C, for 20 hours. The pellet was rinsed with buffer I, and finally resuspended in minimum volume of the same buffer. The ribosome concentration was determined by UV absorbance measurement at 260 nm using conversion coefficient 1 A_{260} unit = 23 pmoles of 70S ribosomes. The prepared ribosome solution was aliquoted, flash-frozen in liquid nitrogen, and stored at -80°C.

Ribosome factors and aminoacyl-tRNA synthetases preparation. *E. coli* His-tagged IF1, IF2, IF3, EF-Tu, EF-G, methionyl- and phenylalanyl-tRNA synthetases were expressed and purified as previously described.(1, 2)

fMet-tRNA^{fMet} preparation. *E. coli* tRNA^{fMet} was overexpressed in BL21 Star (DE3)pLysS cells from a recombinant gene cassette controlled by lpp promoter on pBluescript II SK (+) plasmid (Genscript). After cell lysis by sonication, tRNA^{fMet} was purified on Sepharose 4B column eluted with the reverse gradient of Ammonium Sulfate, and had methionine-accepting activity of 500 pmol/A_{260} unit. The recombinant 6xHis-tagged *E. coli* methionyl-tRNA synthetase and *E. coli* methionyl-tRNA^{fMet} formyltransferase were expressed in BL21 Star (DE3)pLysS cells and purified on HisTrap™ HP 5 ml column according to manufacturer's protocol. The formyl donor, 10-formyltetrahydrofolate, was prepared according to literature.(3) Aminoacylation of tRNA^{fMet} with subsequent formylation of Met-tRNA^{fMet} was performed as a one-pot reaction in a mixture containing 100 mM Tris-HCl (pH 7.6), 4 mM ATP, 20 mM $MgCl_2$, 10 mM KCl, 150 μM L-Methionine, 750 μM neutralized formyl donor, 7 mM BME, 20 μM tRNA^{fMet}, 12 μM methionyl-tRNA synthetase, and 16 μM methionyl-tRNA^{fMet} formyltransferase. The reaction mixture was incubated at 37°C for 1 hour, then acidified with sodium acetate (pH 5.0) added to the final concentration of 0.5 M. fMet-tRNA^{fMet} was purified by successive phenol and chloroform extractions followed by gel-filtration on NAP-10 column (Cytiva) equilibrated with 0.2 M sodium acetate (pH 5.0). Finally, fMet-tRNA^{fMet} was precipitated with ethanol, the precipitate was washed with 70% (v/v) ethanol, air-dried, and dissolved in 2 mM sodium acetate (pH 5.0). The solution was stored at -80°C.

N-Ac-Phe-tRNA$^{Phe}_{yeast}$ preparation. N-Acetyl-Phe-tRNA^{Phe} was prepared from yeast tRNA^{Phe} (Millipore-Sigma, 1000 pmol/A_{260} unit) according to described procedure.(4)

poly(Phe) synthesis assay. poly(U)-dependent synthesis of poly(L-[^{14}C]Phe) was performed in a reaction mixture assembled from three stocks, Initiation Complex (IC) Premix, Elongation Factor (EF) Premix and Aminoacylation (AM) Premix, prepared separately and combined at 1:2:2 volume ratio, respectively. All of the stocks were prepared using TAM_{10} buffer (1x TAM_{10}: 20 mM Tris-HCl, pH 7.5, 10 mM $MgAc_2$, 30 mM NH_4Cl, 70 mM KCl, 0.5 mM EDTA, 7 mM BME (β-mercaptoethanol)). IC Premix contained 1.5x TAM_{10}, 20 mM Tris-HCl, pH 7.5, 2 mg/ml poly-U RNA, 0.4 μM ribosomes, 1.2 μM N-Ac-Phe-tRNA$^{Phe}_{yeast}$, and was preincubated at 37°C for 30 min. EF Premix contained 1x TAM_{10}, 32 mM Tris-HCl, pH 7.5, 4 mM GTP, 4 mM PEP, 100 μg/ml pyruvate kinase, 12 μM EF-Tu, 4 μM EF-G (or no EF-G in a control), and was preincubated at 37°C for 30 min. AM Premix contained 0.8x TAM_{10}, 33 mM Tris-HCl, pH 7.5, 4 mM ATP, 50 μM L-[^{14}C]Phe, 120 A_{260} units/ml *E.coli* total tRNA (charging capacity 180 pmol Phe/A_{260} unit), 10 ng/ml PheRS, and was preincubated at 37°C for 20 min. AM Premix was combined with EF Premix and incubated at 37°C for 5 min, then IC Premix was added to initiate poly(L-[^{14}C]Phe) synthesis. At appropriate time intervals, 12 μl aliquots were withdrawn from the reaction mixture, quenched with 6 μl of stop solution (1 M KOH, 25 mM EDTA), incubated at 37°C for 1 hour to destroy unused [^{14}C]Phe-tRNA, and acidified with 6 μl 1.5 M sodium acetate (pH 4.5). Finally, 20 μl from each processed aliquot was applied onto a Whatman paper filter pre-impregnated with trichloroacetic acid (TCA). The filters were batch-washed with one change of 10% TCA, five changes of ice-cold 5% TCA, one change of ice-cold ethanol, and air-dried at room temperature for 30 min. Radioactivity of the filters was determined in ScintLogic U scintillation liquid (LabLogic) using Hidex 300 SL liquid scintillation counter.

Equilibrium titrations of EF-G with mant-GTP and mant-GDP. Experiments were performed at room temperature (20°C) with samples prepared in Dilution buffer (50 mM Tris-HCl, pH 7.5, 70 mM NH_4Cl, 30 mM KCl, 10 mM $MgCl_2$, 0.5 mM EDTA, 6 mM BME). A titration grid of EF-G (M5, T48E or T48V) and mant nucleotide (mant-GTP or mant-GDP) was created with concentrations of 0, 2, 4, 8, 16, 32 μM EF-G and 0, 2, 4, 8, 16 μM mant nucleotide, respectively. Fluorescence was measured using a DeNovix QFX fluorometer set with excitation wavelengths in 361-389 nm range and fluorescence detection in 435-485 nm range. For each combination of an EF-G variant

and mant nucleotide the titration grid was triplicated, and the fluorescence intensities from the three replicates were averaged. The obtained values were fitted to the following two-variable equation:

$$F(x, y) = C + D * x + A * y + (B - A - D) * (x + y + K_d - \mathrm{sqrt}((x + y + K_d)^2 - 4 * x * y)) / 2$$

where F(x, y) is the fluorescence intensity in relative fluorescence units (RFU), x and y are the concentrations of EF-G and mant nucleotide, respectively, in μM, A is the specific molar fluorescence of free mant nucleotide in RFU/μM, B is the specific molar fluorescence of EF-G*mant nucleotide complex in RFU/μM, C is the background fluorescence in the absence of EF-G and mant nucleotide in RFU, D is the specific molar fluorescence of free EF-G in RFU/μM, and K_d is the dissociation constant for EF-G*mant nucleotide complex in μM.(5) The titration curves are displayed in Figures S10-S15.

Ribosome-induced GTPase activity of EF-G variants. GTPase activity of EF-G variants was measured using Transcreener GDP FI Assay system (BellBrooks Labs) in the end-point assay format.(6) The assay is based on quantification of fluorescent GDP-derived tracer released from its complex with GDP-specific antibody conjugated with a quencher. Upon GTP hydrolysis by EF-G, the produced GDP displaces the tracer from the complex, which causes the increase of fluorescence emission intensity due to de-quenching. GTPase reaction mixture contained 0.75 μM EF-G, 0.125 μM *E. coli* ribosomes, 100 μM GTP, 20 mM Tris-HCl, pH 7.5, 10 mM $MgCl_2$, 40 mM KCl, 0.5 mM EDTA, 4 mM BME. The reaction was initiated by addition of GTP, carried out at 37°C for several time intervals, and stopped by mixing with equal volume of the Stop & Detect solution containing 90 μg/mL GDP-specific antibody and 4 nM Alexa Fluor™ 594-derivatized GDP tracer in 10 mM HEPES-NaOH, 20 mM EDTA, 0.01% Brij-35, pH 7.5. Afterwards, the mixture was incubated at room temperature (20°C) for 1 hour in the dark to allow equilibration between the antibody, tracer, and GDP. The fluorescence intensity was measured using DeNovix QFX Fluorometer with excitation wavelength range between 490-558 nm and emission detection in 560-650 nm range. The background GDP concentration was accounted for by running GTPase reaction in the absence of ribosomes while keeping all other conditions same. Each measurement conditions was repeated at least three times.

EF-G/ribosome co-sedimentation assay. The pre-translocation ribosome complex carrying fMet-Phenyl-$tRNA^{Phe}$ at the A-site and vacant $tRNA^{fmet}$ at the P-site (fMF-pre, 0.4 μM) was

incubated at 37°C for 5 min with 4 mM GTP and 2 μM of either M5, or T48E, or T48V variant of EF-G in TAM_{10} buffer. Afterwards, the concentration of Mg^{2+} in the binding mixtures was adjusted from 10 to 30 mM. The samples were placed on ice, then layered on top of pre-cooled 1.1 M sucrose cushions in TAM_{30}. The ribosomal complexes were pelleted through the sucrose cushion at 750,000xg and 4°C for 3 hours (Hitachi CS150FNX ultracentrifuge with S140AT rotor). Supernatants were carefully removed; each pellet was resuspended in 10 μl of TAM_{10} buffer and resolved in a 10% SDS PAGE gel (200V/1hr). The gel was stained with Coomassie Brilliant Blue R-250, destained with 20% (v/v) ethanol, 5% (v/v) acetic acid, and photographed using ChemiDoc Touch Imaging System (Bio-Rad).

Multiple sequence alignment of P-loop/switch 1 regions. Several representative EF-G/EF2 proteins are aligned: EFG_ECOLI, EF-G from E. coli strain K-12; EFG_STAAC, EF-G from Staphylococcus aureus strain COL; EFG_SYNP2, EF-G from Synechococcus sp. strain ATCC 27264 / PCC 7002 / PR-6 (Agmenellum quadruplicatum); EF2_YEAST, eEF2 from Saccharomyces cerevisiae strain ATCC 204508 / S288c; EF2_RABIT, eEF2 from Oryctolagus cuniculus; EF2_HUMAN, eEF2 from Homo sapiens. Position numbering of EFG_ECOLI, EF2_YEAST, EF2_RABIT, and EF2_HUMAN corresponds to the mature protein sequences with removed N-terminal methionine residue. Position numbering of EFG_STAAC and EFG_SYNP2 is derived from the corresponding gene sequences with retention of the N-terminal methionine. The sequences were aligned using SeaView software and further refined with structurally validated corrections. Boundaries of the P-loop and switch 1 are given according to Pulk A et al.(7)

Table S1. Particle counts in FRET efficiency histograms.

Figure ID	1E	1F	1G	1H		
Particle counts	1015	4779	3161	1827		
Figure ID	2A	2D	2B	2E	2C	2F
Particle counts	731	1827	2779	1191	461	1843
Figure ID	5A	5B	5C	5D	5E	
Particle counts	1930	1201	1015	3161	1827	
Figure ID	5F	5G	5H	5I	5J	
Particle counts	8913	1491	3078	3176	2328	
Figure ID	5K	5L	5M	5N	5O	
Particle counts	889	720	885	5929	2326	
Figure ID	S2					
Particle counts	626					

Table S2. Fitted Gaussian positions (xo) and standard deviations (σ) for Figure 2. Values were calculated using the equation f(x)=Ae^(-〖(x-x_o)〗^2/〖2σ〗^2) in MathCad. All values were fit using a singular fitting.

	L27-tRNA x_o	L27-tRNA σ	EF-G x_o	EF-G σ
GTP pre-complex	0.366	±0.093	0.483	±0.085
GDP pre-complex	0.347	±0.077	0.657	±0.080
GDPCP pre-complex	0.408	±0.069	0.540	±0.065
GTP post-complex	0.544	±0.105	0.490	±0.111
GDP post-complex	0.533	±0.086	0.713	±0.079
GDPCP post-complex	0.520	±0.086	0.573	±0.074

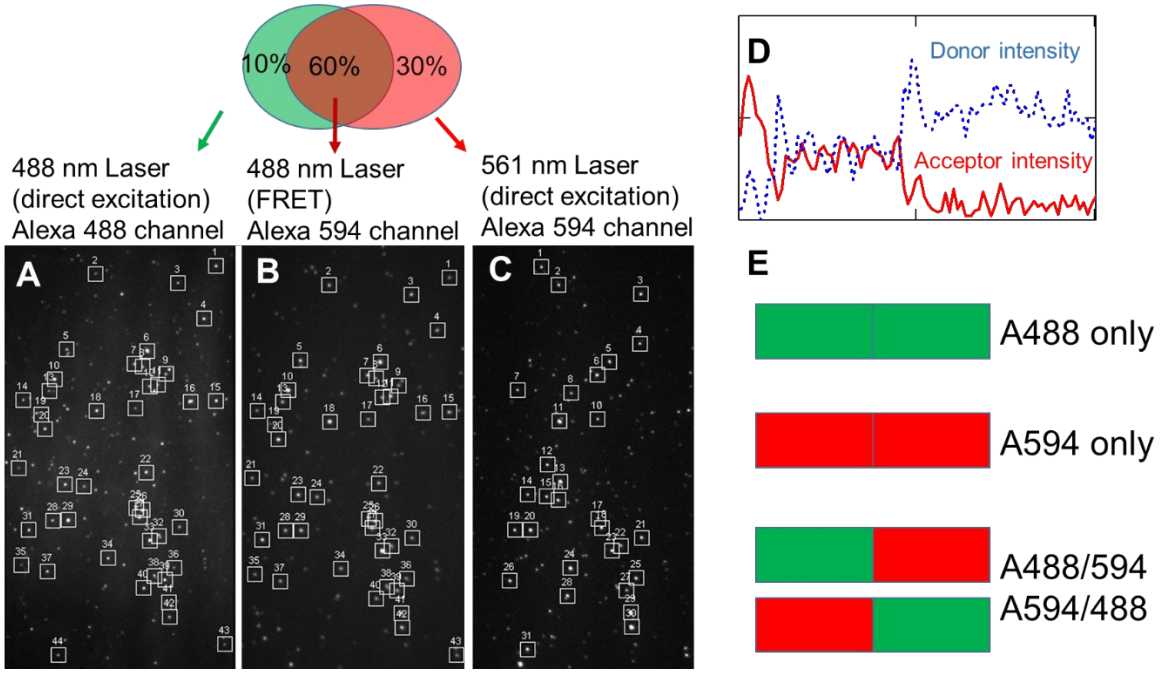

Figure S1. Analysis of Labeling composition of EF-G. (A-B) One image frame taken from a single movie showing directly excited Alexa 488 dye and FRET-excited Alexa 594 via a 488 nm laser, respectively. **(C)** One frame taken from a single movie showing directly excited Alexa 594 dye via a 561 nm laser. All images in A-C are from the same field of view. Squares show FRET pairs with ImageJ program. **(D)** Example of fluorescence emission intensities of the Alexa 488 (blue trace) and the Alexa 594 (red trace) over time. **(E)** Possibilities of the two cysteine labeling sites: both Alexa 488, both Alexa 594, or a combination of the two dyes. About 10% of labeling sites are Alexa 488 double labeled, 60% are a combination of Alexa 488/594, and 30% are Alexa 594 double labeled (detail of the analysis is given below).

The two unique cysteines at positions F410C and Y533C were simultaneously labeled with mono-maleimide Alexa Fluor™ 488 (A488) and 594 (A594). Assuming equal labeling efficiency on both residues, three labeling compositions were possible: both A488, both A594, or (A488/594 or A594/488) (**Fig. S1E**). The compositions were measured via smFRET- and direct-excitations of the acceptor (A594). In the smFRET-excitation experiments, the 488 nm laser excited the A488 directly, which emitted in the A488 channel (**Fig. S1A**). Meanwhile, A594 emitted in the A594 channel via FRET (**Fig. S1B**) only if it was co-labeled on the same EF-G. The FRET pairs were fit with imageJ program (**Fig. S1C**). Therefore, the numbers of emitters in A488 and A594 channels corresponded to numbers of EF-G labeled with at least one A488 and

double labeled with A488/594, respectively. Similarly, the number of EF-G labeled with at least one A594 was measured by emissions in the A594 channel under 560 nm laser (**Fig. S1C**), which only excited the A594 but not A488 dye. Consequently, the labeling composition can be represented as the overlapped ovals in the plot, in which the green and red ovals represented the EF-G being labeled with at least one Cy3 and Cy5, respectively; and the overlapped area represented the double labeled EF-G. The percentage of the EF-G labeled with A488/594 or A594/488 on C410/C534, respectively, was estimated to be approximately 60% (±7%, average of 300 field of views). The FRET efficiency histogram did not exhibit two peaks (**Fig. S3A**). Therefore, the mixture of double labeled EF-G (A488/A594 or A594/A488) was treated as one species. Other labeling components did not interfere with the FRET-data analysis because A594-only labeled EF-G did not generate any signal, and in the meantime A488-only labeled EF-G was not picked by the FRET-pair seeking program.

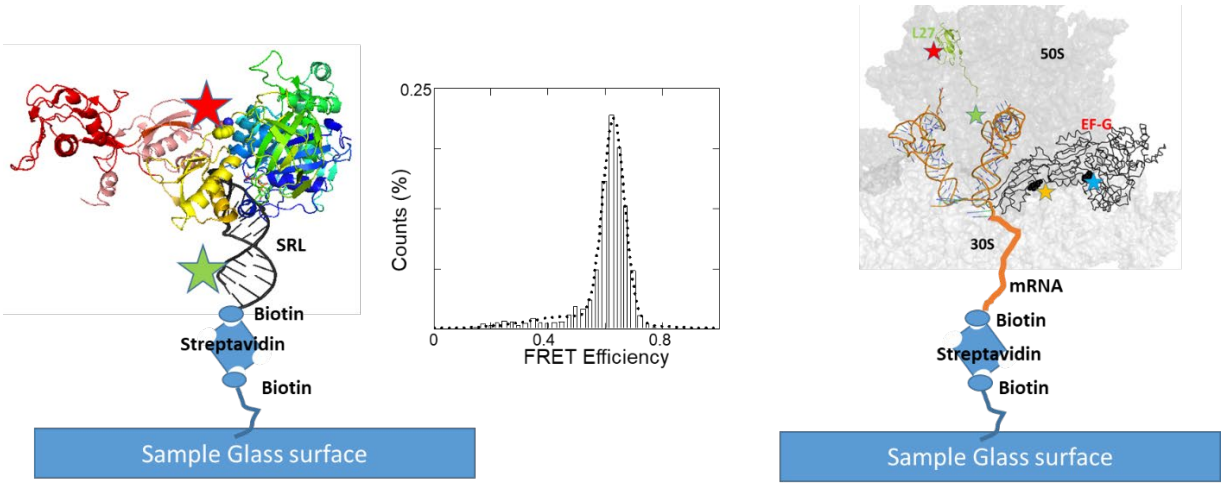

Figure S2. Surface tethering and FRET labeling strategies for SRL/Ribosome – EF-G complexes. The FRET efficiency histogram shows close proximity of 5'-biotin-SRL-3'-Cy5 to the EF-G labeled at F410C position with Cy3 dye, indicating proper interaction between the two molecules. Stars showed the positions of dye labeling. The particle counts for the FRET efficiency histograms can be found in **Table S1**.

A

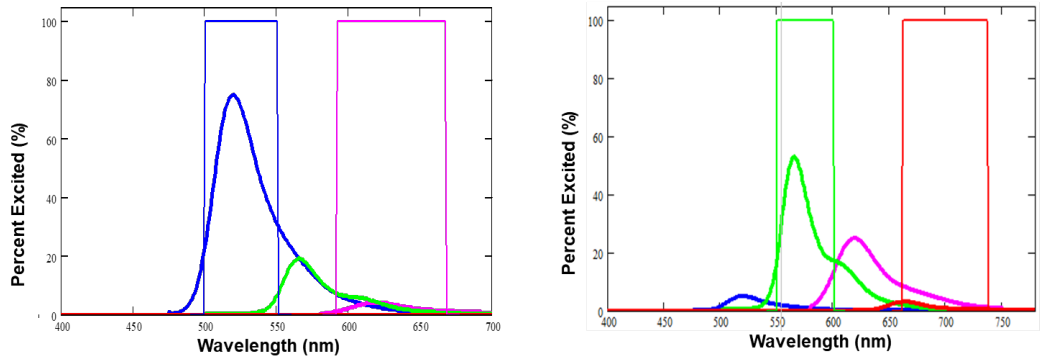

B

Fluorescent Dye	A488 (3788)	A594 (244.9)	Cy3 (2384)	Cy5 (149.1)
500-550 nm	2735	0	47	0
592-667 nm	177	195	244	0
550-600 nm	51	125	1716	0
662-737 nm	0.4	310	47	95.3

Figure S3. Crosstalk correction procedure for dual channel smFRET experiments. (A) Fluorescence emission spectra of all fluorophores under 488 nm (left) or 532 nm (right) laser excitation. The intensities are corrected by laser absorption and quantum yields. Colored rectangles show filters used for the Alex488 (blue)/Alexa594 (magenta) and Cy3 (green)/Cy5 pairs (red), respectively. **(B)** Relative fluorescence intensities for dyes within the filters as shown in **(A)**. The intensities are scaled by excitation efficiencies under the specific laser line, after considering the absorption and emission yields (https://www.thermofisher.com/order/fluorescence-spectraviewer#!/).

Crosstalk between laser wavelengths and filter sets was observed during multi-channel smFRET experiments. There were undesired direct excitations and spectrum crosstalks. For example, in **Figure S3A**, Cy3 direct excitation (green trace) by 488 nm laser spilled over into 488/594 FRET filter windows (blue and magenta rectangles). Similarly, Alexa 488 and Alexa 594 dyes were direct excited by 532 nm laser and bled into Cy3/Cy5 FRET filter windows (green and red rectangles). The composition of signal in each channel under both laser excitations were tabulated in **Figure S3B** and deconvoluted in FRET calculation. The values in **Figure S3B** are the integration area beneath the fluorescence emission spectra defined by the filter boundaries. The values in the parenthesis are the total area for each fluorescence curve.

Deconvolution for Alexa488/594 FRET pair under 488 nm laser excitation: The second and third rows in the above table indicate that the sum of fluorescence intensities from both the donor and acceptor channels is 2735 + 47 + 177 + 195 + 244, totaling 3398. According to FRET theory, even though the intensities of the donor and acceptor can change due to energy transfer, their combined fluorescence should always match the initial intensity of the donor alone. To illustrate, a FRET efficiency of 50% would result in 50% * 2735 in the donor channel and the same amount in the acceptor channel. Similarly, a 20% FRET efficiency would yield 80% * 2735 in the donor channel and 20% * 2735 in the acceptor channel. In each scenario, the combined fluorescence from the two channels remains unchanged, regardless of the FRET efficiency. By considering this combined fluorescence, the variable FRET signals across donor and acceptor channels are eliminated from the formula. For clarity, 'SUM' denotes the experimental total fluorescence intensities of both channels, while 'D' and 'A' represent the experimental fluorescence intensity in the donor and acceptor channels, respectively. Consequently, I_{A488} = D-SUM*47/3398 = D-SUM*1.38%. Here, deconvolute with “SUM*47/3398” is more accurate than use “D*47/2735” because the area 2735 represent the theoretical total energy that will be partitioned between the donor and acceptor, while D is the experimental value after FRET occurred. Given that the experimental D value doesn't scale linearly with the theoretical 2735 value due to energy transferred away to the acceptor, the contamination from Cy3 isn't proportionate to the 47/2735 factor. However, irrespective of FRET, the combined energy from both the donor and acceptor channels should align proportionally with the theoretical sum values, as we elaborated above. As a result, the scaling factors are determined using the SUM as the denominator. Similarly, I_{A594} = A-SUM*(177+195+244)/3398=A-SUM*18%. So FRET is calculated by (I_{A594})/(I_{A594} + I_{A488}) = **(82%*A-18%D)/(SUM*81.6%)**

Deconvolution for *Cy3*/*Cy5* FRET pair under *532* nm laser excitation: *Using similar formula,* I_{Cy3} = D-SUM*(51+125)/2280.7 = D-SUM*7.7%. Similarly, I_{Cy5} = A-SUM*(0.4+310+47+95.3)/2280.7=A-SUM*20%. So FRET is calculated by (I_{Cy5})/(I_{Cy5} + I_{Cy3}) = **(80%*A-20%D)/(SUM*72.3%)**

Figure S4. Examples of extended and compact EF-G conformations. (A) Overlay of free EF-G (1fnm, cyan) and ribosome bound EF-G (7pjv, magenta). **(B-C)** The extension of the domain VI is accompanied by an increased distance between domain I and V. The residues 410 and 533 are depicted in spheres form.

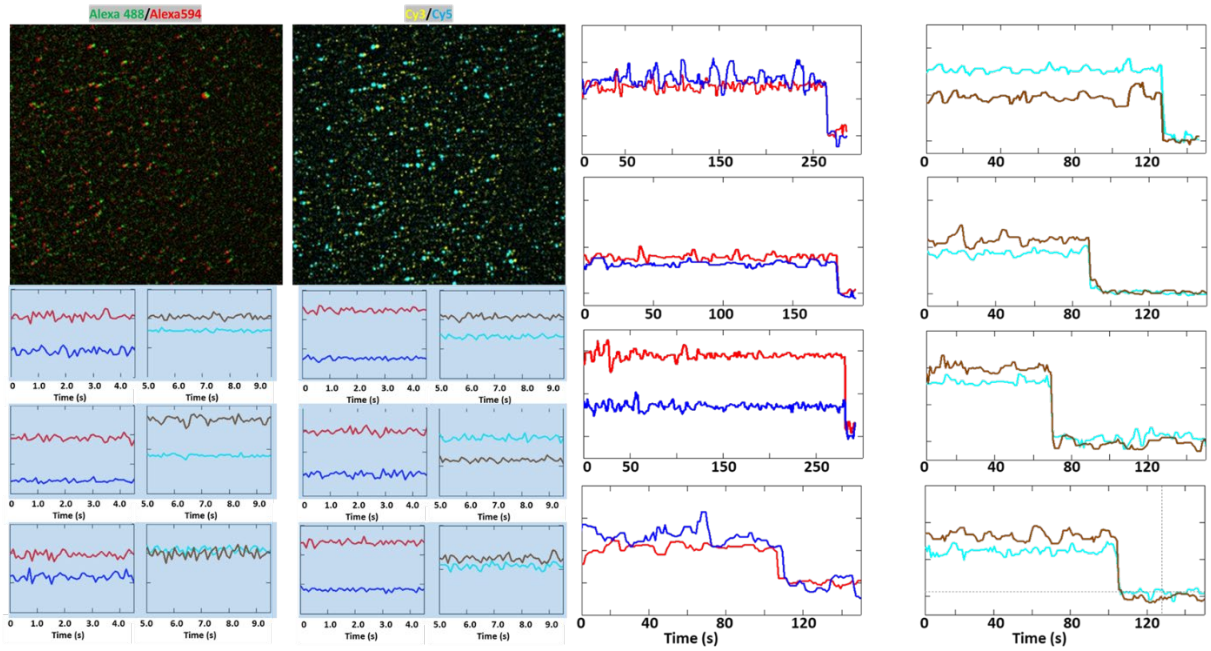

Figure S5. Representative image and fitted fluorescence intensity traces from Figure 5J histogram (total particles 2328). Red/Blue: Alexa 488/Alexa 594; Brown/Cyan: Cy3/Cy5.

Figure S5 displays some representative smFRET images and some fitted traces. Single step bleaching traces were collected at prolonged time-lapse, and 10x higher laser power (400 mW) was exerted to bleach the Cy3/Cy5 FRET pair.

The left camera image shows an overlay emission of Alexa488/Alex a594 that are labeled on EF-G, while the right camera image is an overlay emission of Cy3/Cy5 that are labeled on tRNA/L27 (time-lapse traces are shorted for display clarity). They are the same ribosome complexes at the matching coordinates. These images are stacked into one movie, and the fluorescence intensities were fitted in one trace of 100 time points, in which the first 50 points reflect signals from the Alexa488/Alexa594 channels, and the subsequent 50 points depict signals from the Cy3/Cy5 channels. The single molecule particles are selected by program with consistent parameters. The selection criteria mirror those previously described (1). Specifically, intensity values are confined between 100 and 2000, and the signal-to-noise ratio (S/N) must exceed 4. Traces that meet these stipulations across all four channels are chosen for further analysis. For instance, in **Figure 5J**, 6626 particles were chosen from the EF-G FRET images based on the first 5 seconds of the fitted traces. Of these, 2328 particles demonstrated signals surpassing the threshold from the Cy3/Cy5 FRET images during the subsequent 5 seconds.

Consequently, the histogram was compiled from this final collection of 2328 particles. The particle counts for the FRET efficiency histograms can be found in **Table S1**.

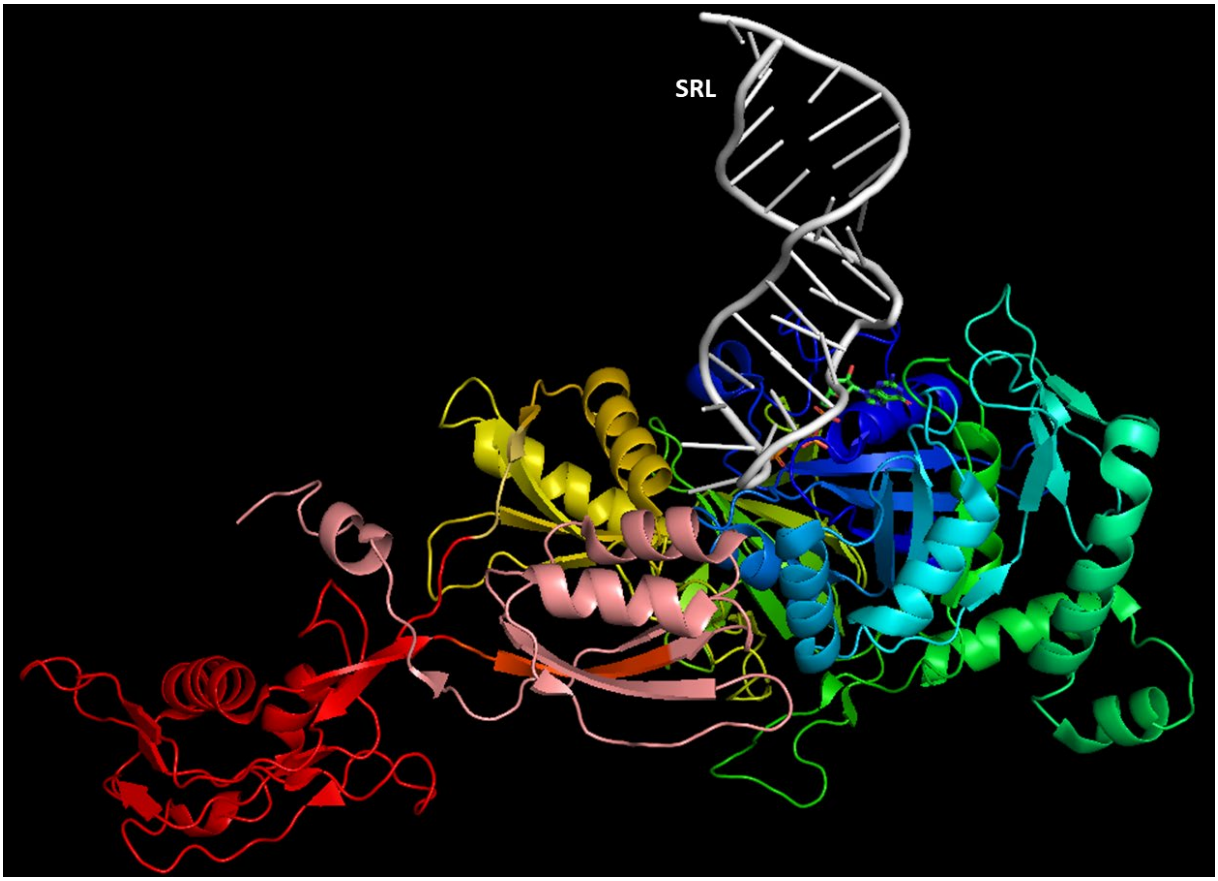

Figure S6. Interaction of SR loop with the EF-G (based on structure 7pjv).

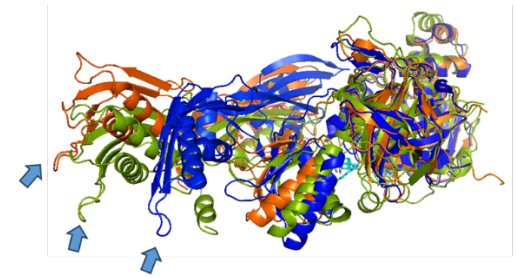

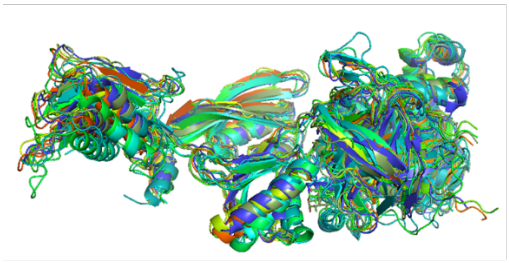

ID	ribosome	tRNA	nucleotide
4v5f	post	$tRNA^{fmet}$ P/P $tRNA^{fmet}$ E/E	GTP•Fus
3j9z	post	$tRNA^{Leu}$ P/P $tRNA^{fmet}$ E/E	GTP/GDPPi
1fnm	no		GDP

ID	ribosome	tRNA	nucleotide
4wqf	post	fmet-$tRNA^{fmet}$ P/P fmet-$tRNA^{fmet}$ E/E	GDP•Fus
4v5f	post	$tRNA^{fmet}$ P/P $tRNA^{fmet}$ E/E	GDP•Fus
4v9h	int	$tRNA^{Phe}$ P/E	GDPCP
4v9k	int	$tRNA^{fmet}$ PE*/E	GDPNP
4v9o	int	none	GDPCP
4v9L	int	$tRNA^{fmet}$ PE*/E	GDP•Fus
7pjv	pre	fMet-phe-$tRNA^{Phe}$ A/P $tRNA^{fMet}$ P/E	GDP•Pi
4w29	int	Acetyl-Val-$tRNA^{Val}$ AP/AP site $tRNA^{fMet}$ PE/E	GDP•Fus

Figure S7. Structure variations of EF-G in bound and free forms (1fnm). The top panel overlaid three representative structures of EF-G, with increasing distances between the domain IV and domain III, in the order of 1fnm, 3j9z, and 4v5f. The bottom panel showcases some of the representative bound EF-G complexes with similar extended conformation, irrespective of tRNA and nucleotide configurations.

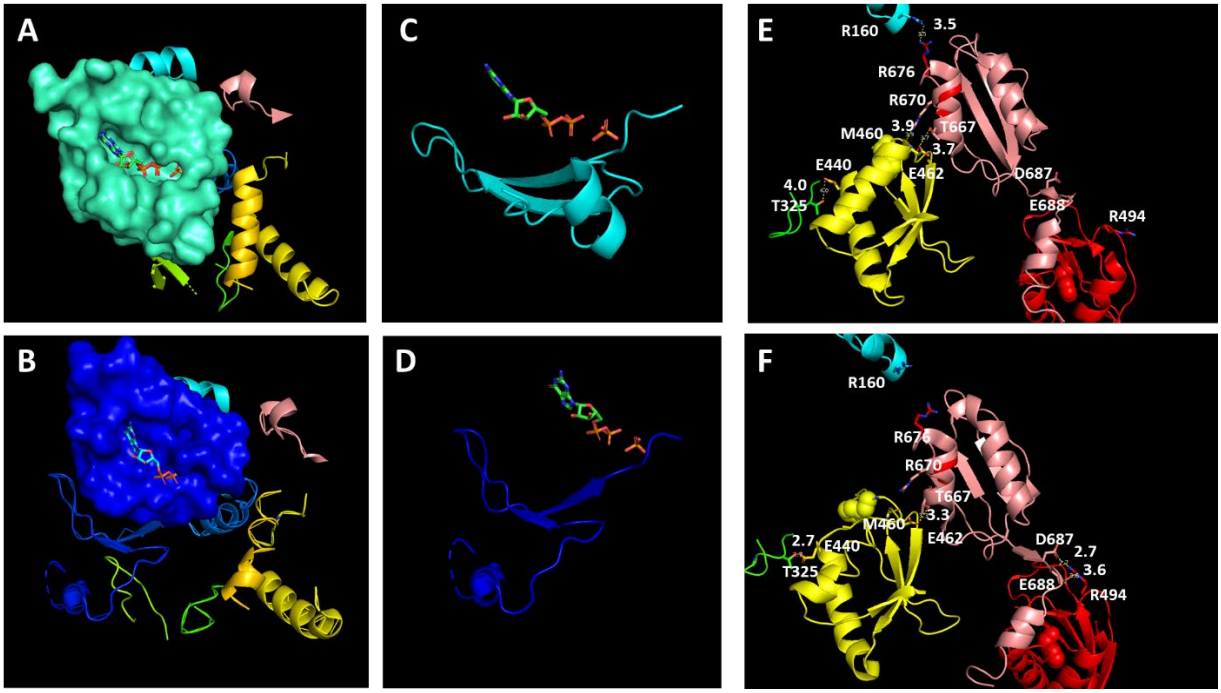

Figure S8. (A) The closed GTP binding pocket before Pi releasing but after GTP hydrolysis (7pjv). **(B)** The opened GTP binding pocket after Pi releasing (7pjy). **(C)** The effect loop and GDP•Pi in the closed form. **(D)** The effect loop and GDP•Pi in the opened form. The Pi is overlay from (C). **(E-F)** Interdomain interactions of domain III (yellow), IV (red) and V (salmon) to show the molecular rearrangement during the opening process. Some of the residues are shown to break or form interdomain H-bondings.

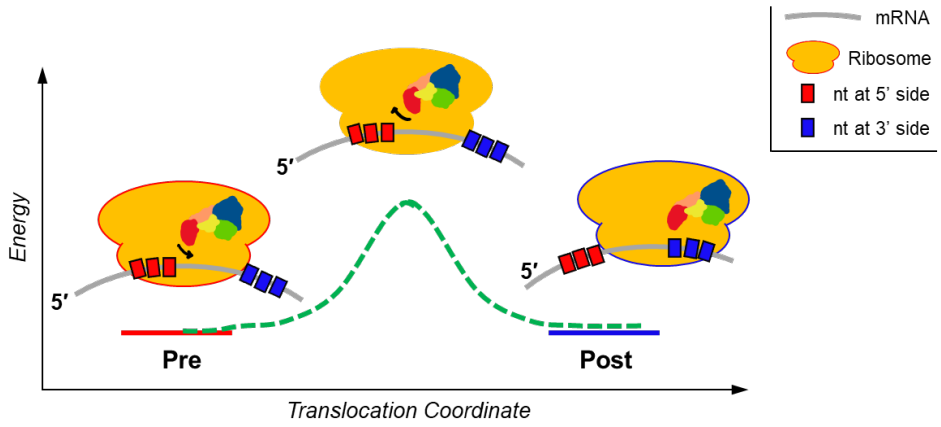

Figure S9. A illustration of the possible role of the highly compact EF-G during translocation.

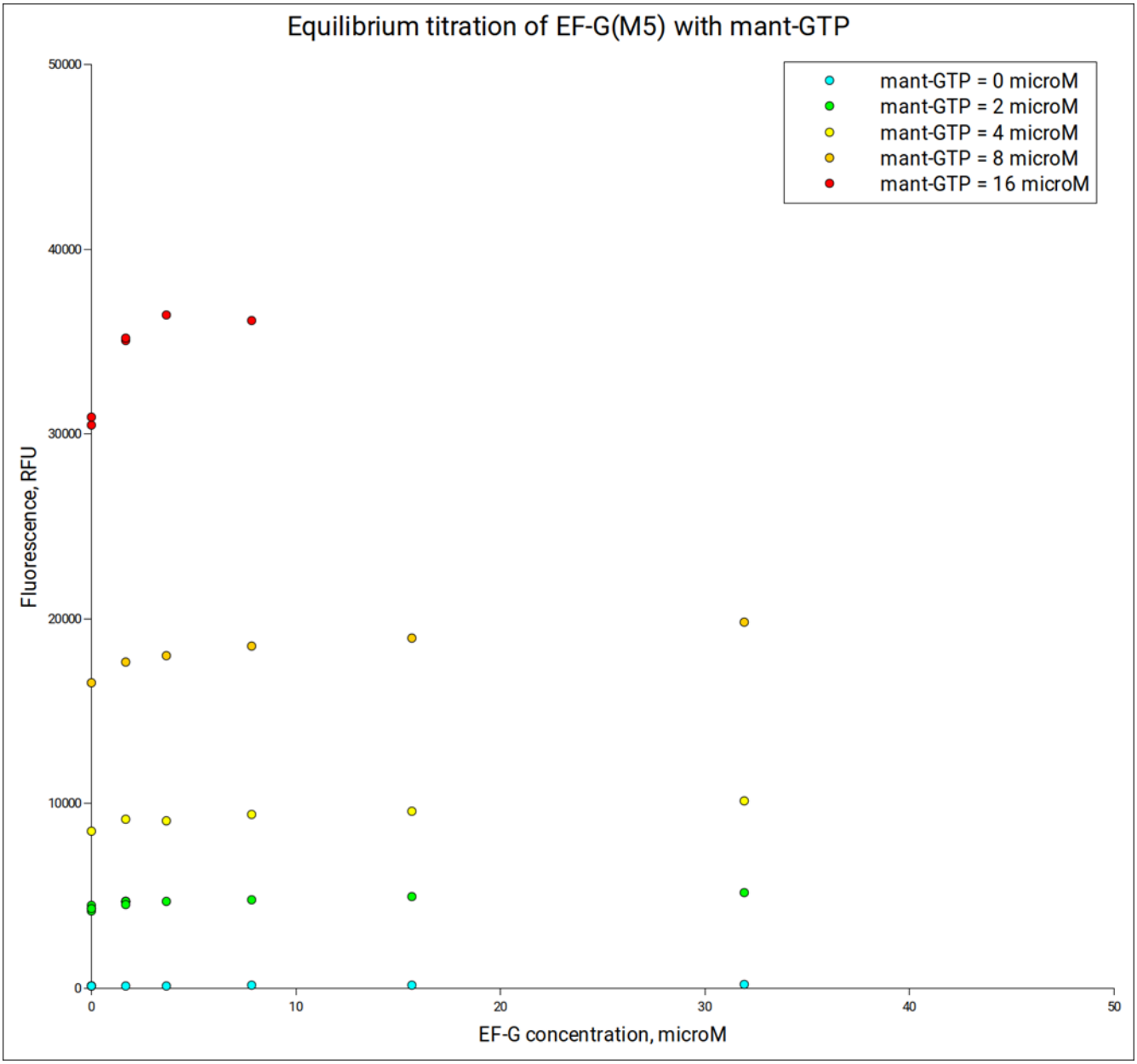

Figure S10. Equilibrium titration of EF-G (M5) with mant-GTP. Experiments were performed at room temperature (20°C) with samples prepared in Dilution buffer (50 mM Tris-HCl, pH 7.5, 70 mM NH4Cl, 30 mM KCl, 10 mM MgCl2, 0.5 mM EDTA, 6 mM 2-mercaptoethanol). Fluorescence was measured using a DeNovix QFX fluorometer set with excitation wavelengths in 361-389 nm range and fluorescence detection in 435-485 nm range. Each plotted value represents an average of three measurements.

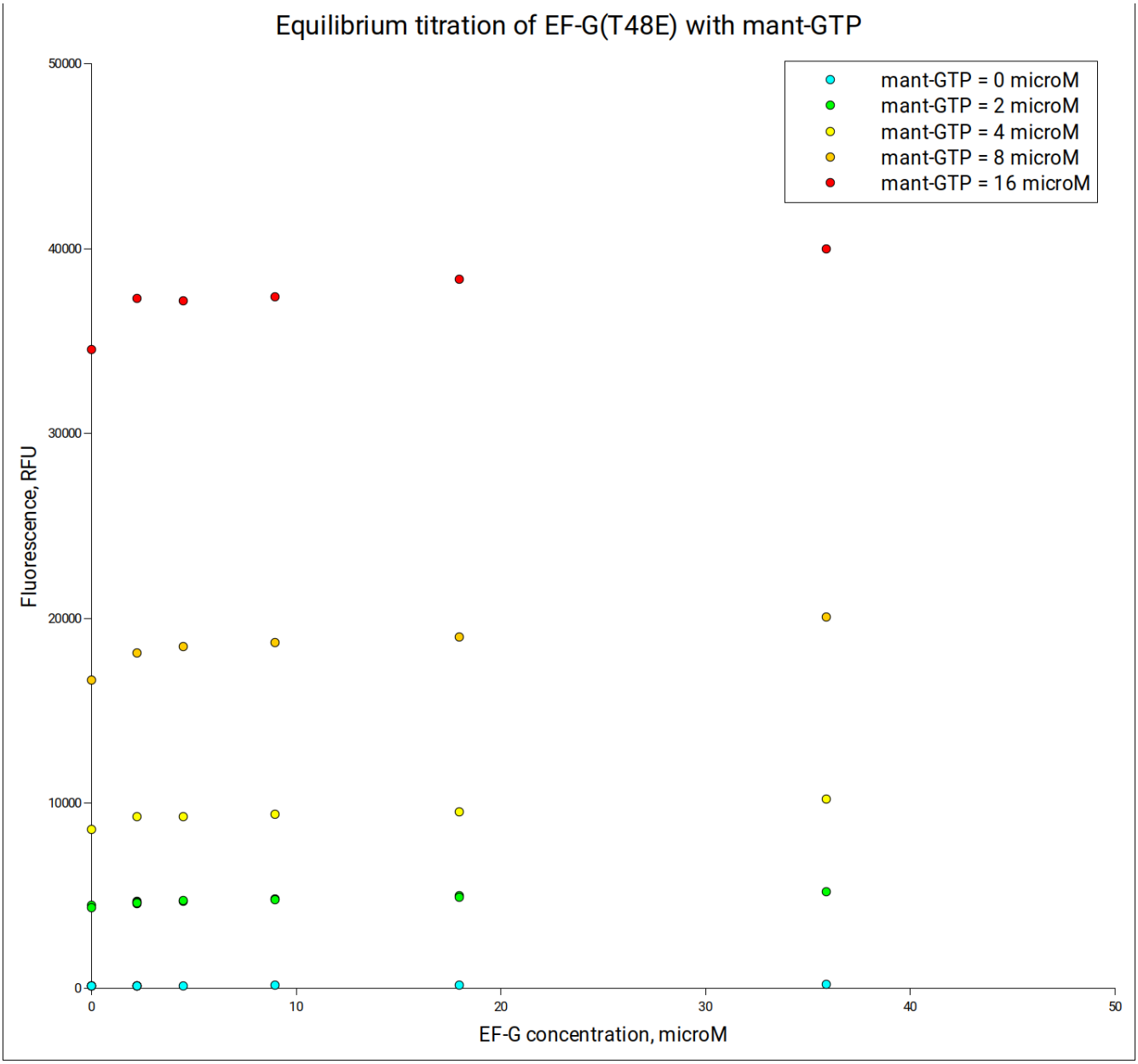

Figure S11. Equilibrium titration of EF-G (T48E) with mant-GTP. Experiments were performed at room temperature (20°C) with samples prepared in Dilution buffer (50 mM Tris-HCl, pH 7.5, 70 mM NH4Cl, 30 mM KCl, 10 mM MgCl2, 0.5 mM EDTA, 6 mM 2-mercaptoethanol). Fluorescence was measured using a DeNovix QFX fluorometer set with excitation wavelengths in 361-389 nm range and fluorescence detection in 435-485 nm range. Each plotted value represents an average of three measurements.

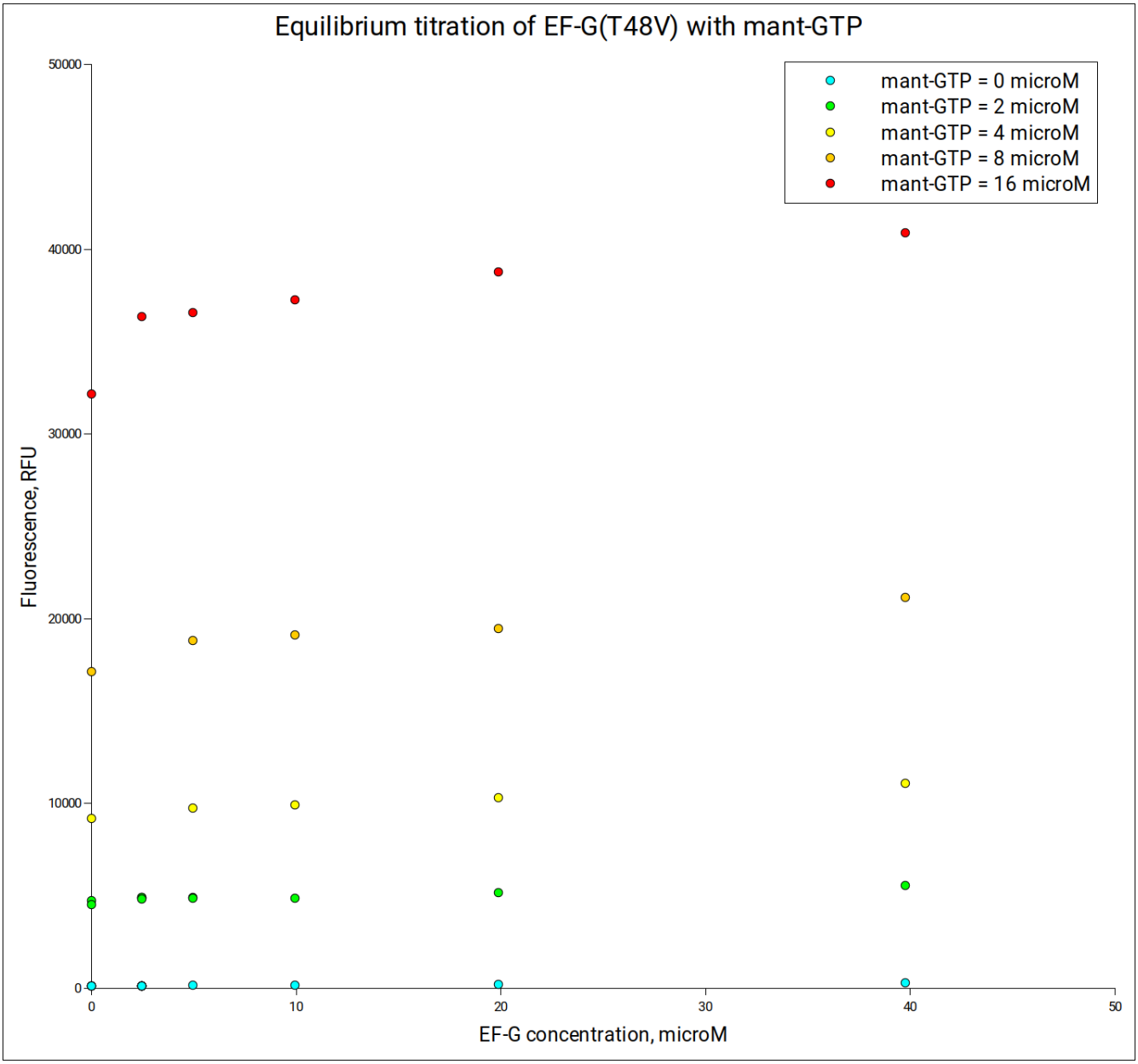

Figure S12. Equilibrium titration of EF-G (T48V) with mant-GTP. Experiments were performed at room temperature (20°C) with samples prepared in Dilution buffer (50 mM Tris-HCl, pH 7.5, 70 mM NH_4Cl, 30 mM KCl, 10 mM $MgCl_2$, 0.5 mM EDTA, 6 mM 2-mercaptoethanol). Fluorescence was measured using a DeNovix QFX fluorometer set with excitation wavelengths in 361-389 nm range and fluorescence detection in 435-485 nm range. Each plotted value represents an average of three measurements.

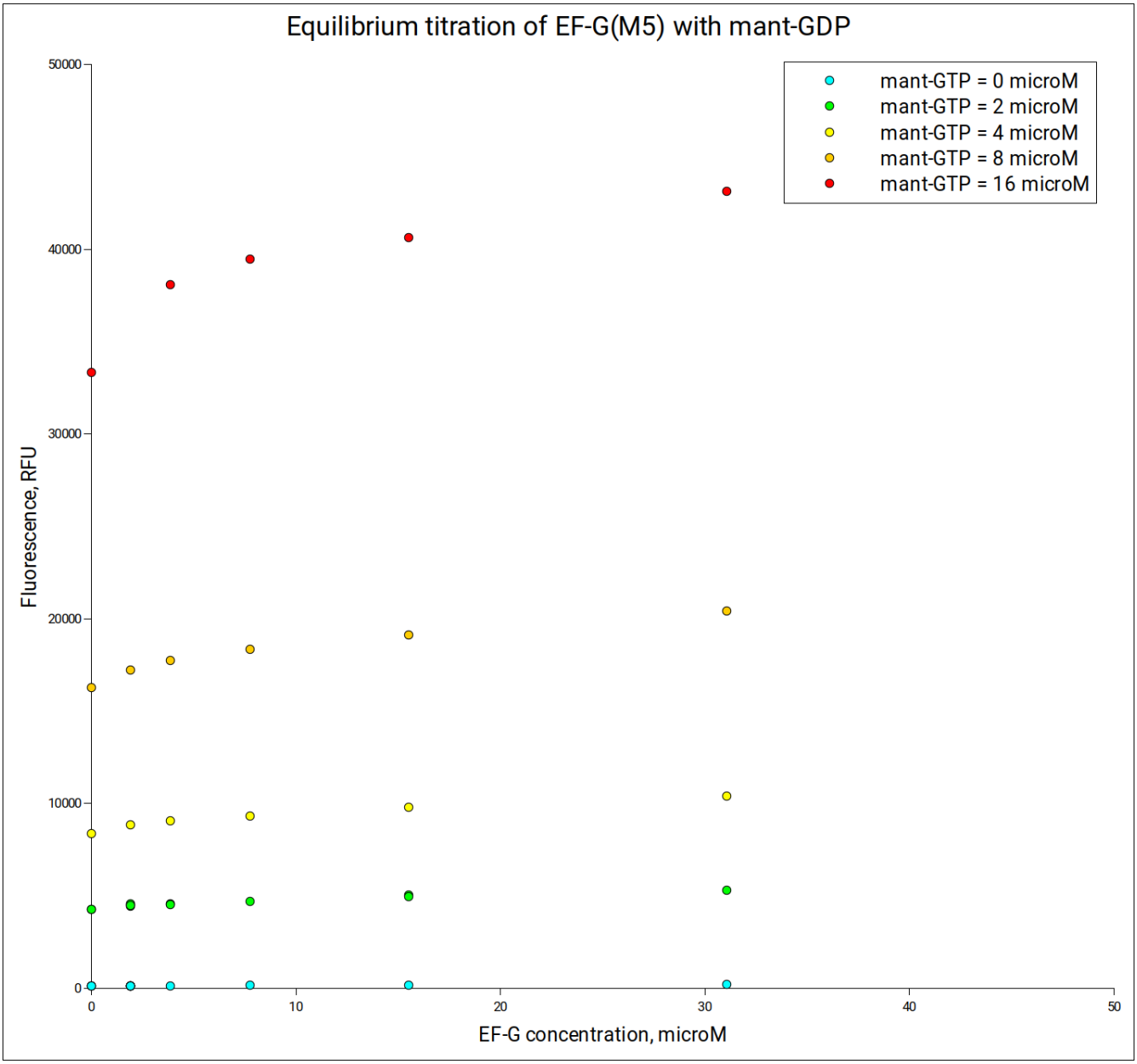

Figure S13. Equilibrium titration of EF-G (M5) with mant-GDP. Experiments were performed at room temperature (20°C) with samples prepared in Dilution buffer (50 mM Tris-HCl, pH 7.5, 70 mM NH_4Cl, 30 mM KCl, 10 mM $MgCl_2$, 0.5 mM EDTA, 6 mM 2-mercaptoethanol). Fluorescence was measured using a DeNovix QFX fluorometer set with excitation wavelengths in 361-389 nm range and fluorescence detection in 435-485 nm range. Each plotted value represents an average of three measurements.

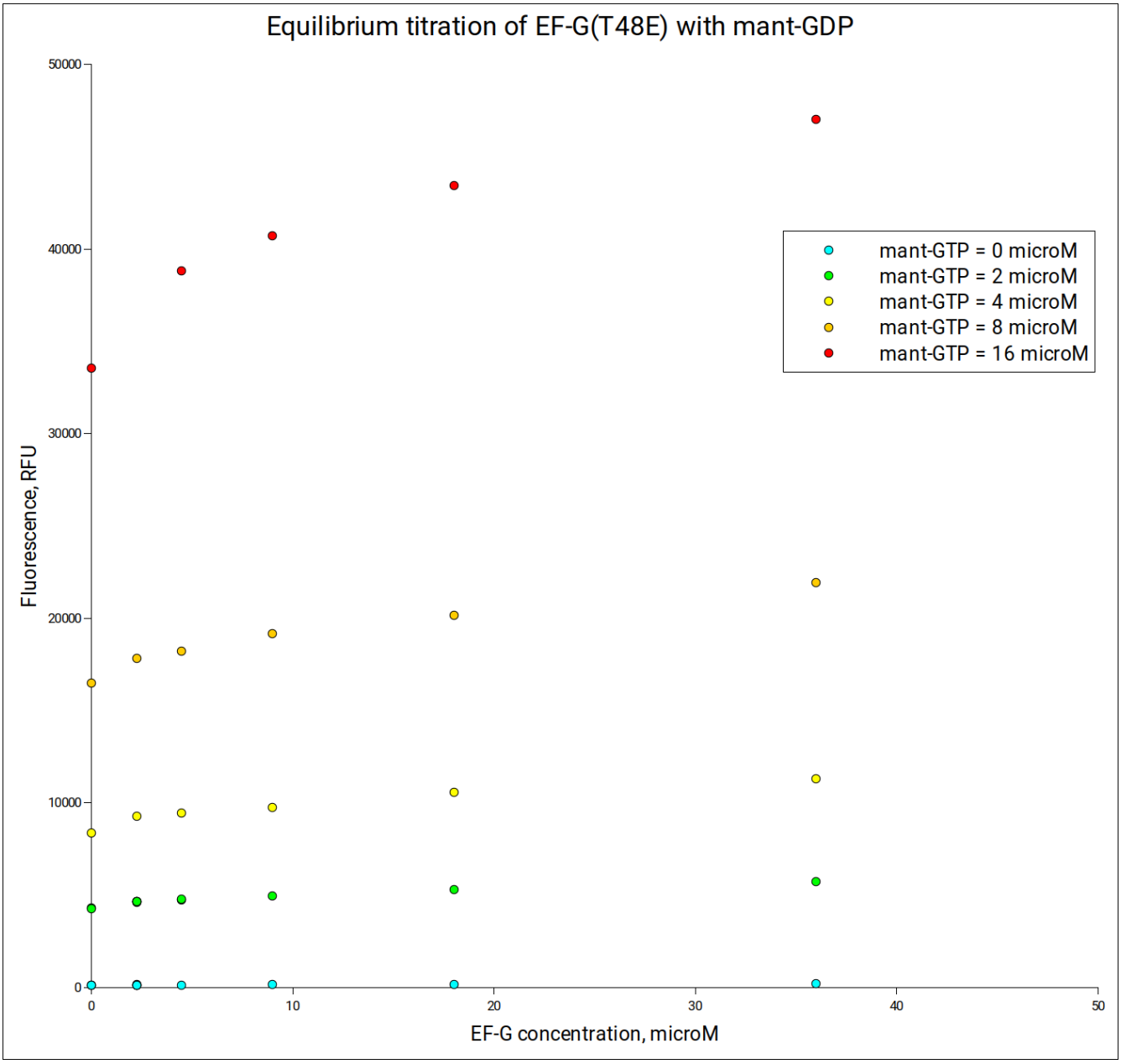

Figure S14. Equilibrium titration of EF-G (T48E) with mant-GDP. Experiments were performed at room temperature (20°C) with samples prepared in Dilution buffer (50 mM Tris-HCl, pH 7.5, 70 mM NH_4Cl, 30 mM KCl, 10 mM $MgCl_2$, 0.5 mM EDTA, 6 mM 2-mercaptoethanol). Fluorescence was measured using a DeNovix QFX fluorometer set with excitation wavelengths in 361-389 nm range and fluorescence detection in 435-485 nm range. Each plotted value represents an average of three measurements.

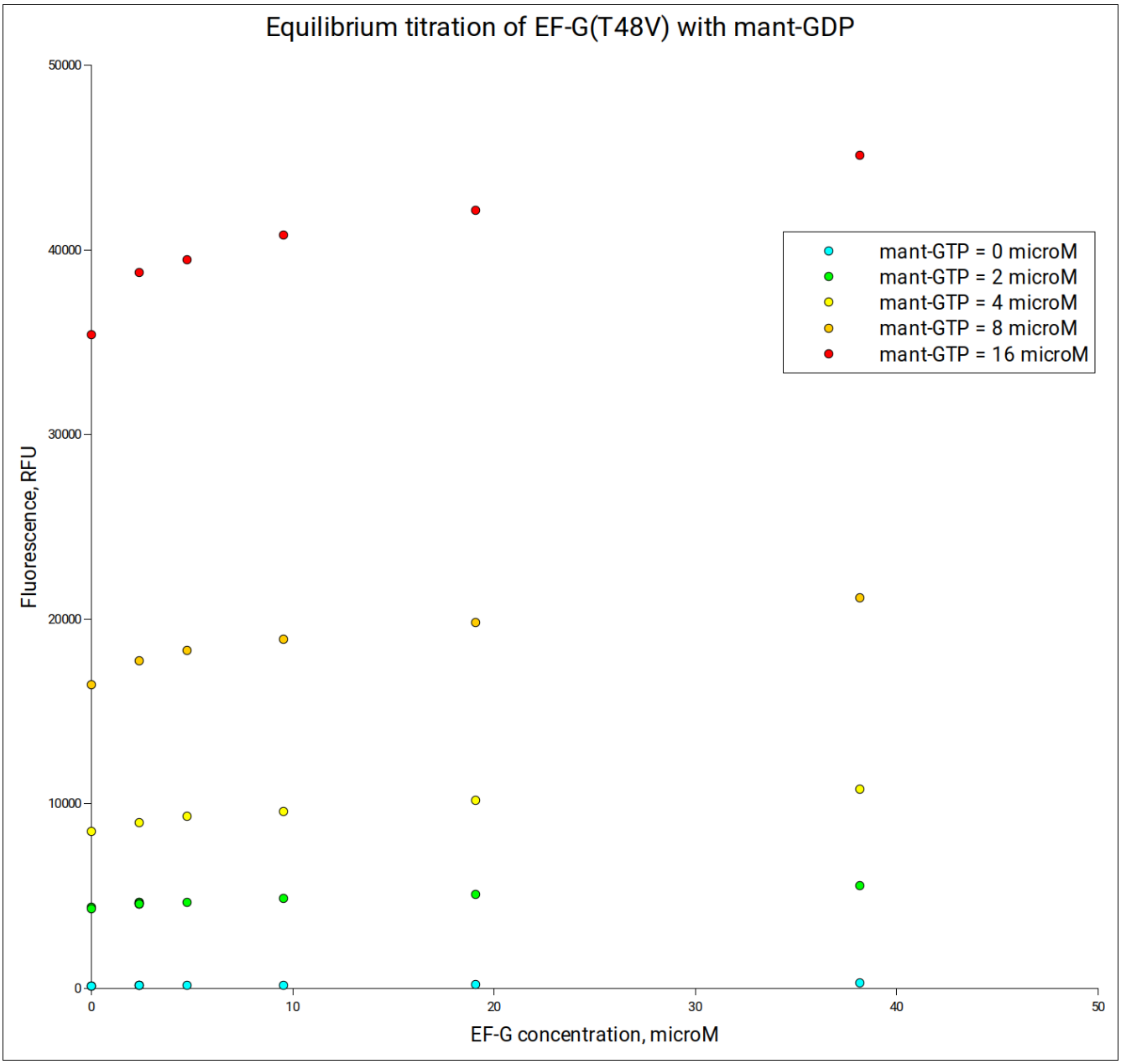

Figure S15. Equilibrium titration of EF-G (T48V) with mant-GDP. Experiments were performed at room temperature (20°C) with samples prepared in Dilution buffer (50 mM Tris-HCl, pH 7.5, 70 mM NH_4Cl, 30 mM KCl, 10 mM $MgCl_2$, 0.5 mM EDTA, 6 mM 2-mercaptoethanol). Fluorescence was measured using a DeNovix QFX fluorometer set with excitation wavelengths in 361-389 nm range and fluorescence detection in 435-485 nm range. Each plotted value represents an average of three measurements.

Reference

1. M. E. Altuntop, C. T. Ly, Y. Wang, Single-molecule study of ribosome hierarchic dynamics at the peptidyl transferase center. *Biophysical journal* **99**, 3002-3009 (2010).
2. T. W. Tsai, H. Yang, H. Yin, S. Xu, Y. Wang, High-Efficiency "-1" and "-2" Ribosomal Frameshiftings Revealed by Force Spectroscopy. *ACS chemical biology* **12**, 1629-1635 (2017).
3. J. S. Dubnoff, U. Maitra, Isolation and properties of polypeptide chain initiation factor FII from Escherichia coli: evidence for a dual function. *Proc Natl Acad Sci U S A* **68**, 318-323 (1971).
4. A. L. Haenni, F. Chapeville, The behaviour of acetylphenylalanyl soluble ribonucleic acid in polyphenylalanine synthesis. *Biochim Biophys Acta* **114**, 135-148 (1966).
5. B. Wilden, A. Savelsbergh, M. V. Rodnina, W. Wintermeyer, Role and timing of GTP binding and hydrolysis during EF-G-dependent tRNA translocation on the ribosome. *Proc Natl Acad Sci U S A* **103**, 13670-13675 (2006).
6. J. Verhelst *et al.*, Functional Comparison of Mx1 from Two Different Mouse Species Reveals the Involvement of Loop L4 in the Antiviral Activity against Influenza A Viruses. *J Virol* **89**, 10879-10890 (2015).
7. A. Pulk, J. H. Cate, Control of ribosomal subunit rotation by elongation factor G. *Science* **340**, 1235970 (2013).